

Towards explaining the generalization gap in neural networks using topological data analysis

Rubén Ballester^{a,b,*}, Xavier Arnal Clemente^a, Carles Casacuberta^{a,1}, Meysam Madadi^b, Ciprian A. Corneanu^c, Sergio Escalera^{a,b,2}

^a*Departament de Matemàtiques i Informàtica, Universitat de Barcelona*

^b*Computer Vision Center, Universitat Autònoma de Barcelona*

^c*Amazon*

Abstract

Understanding how neural networks generalize on unseen data is crucial for designing more robust and reliable models. In this paper, we study the generalization gap of neural networks using methods from topological data analysis. For this purpose, we compute homological persistence diagrams of weighted graphs constructed from neuron activation correlations after a training phase, aiming to capture patterns that are linked to the generalization capacity of the network. We compare the usefulness of different numerical summaries from persistence diagrams and show that a combination of some of them can accurately predict and partially explain the generalization gap without the need of a test set. Evaluation on two computer vision recognition tasks (CIFAR10 and SVHN) shows competitive generalization gap prediction when compared against state-of-the-art methods.

1. Introduction

Understanding the generalization capacity of a neural network is one of the most important questions in deep learning. Unfortunately, while the fundamental procedures of training neural networks are well understood, being able to tell why one network is better at generalizing than another still poses a great challenge. Good performance of a deep neural network (DNN) depends fundamentally on its architecture and its neuron functions and parameters. These yield an approximation of the desired function (prediction or regression) based on neuron interactions—the better the approximation, the better the generalization. However, with the high quantity of neurons and connections of deep neural networks (sometimes of the order of millions), understanding which interactions between neurons are improving or damaging a model is a hard problem. Developing new mathematical tools that capture the effect of these interactions on the output of the networks is key for increased understanding of network generalization.

*Corresponding author

Email addresses: ruben.ballester@ub.edu (Rubén Ballester), xavi.aclm@gmail.com (Xavier Arnal Clemente), carles.casacuberta@ub.edu (Carles Casacuberta), meysam.madadi@gmail.com (Meysam Madadi), cipriancorneanu@gmail.com (Ciprian A. Corneanu), sergio.escalera.guerrero@gmail.com (Sergio Escalera)

¹Partially supported by MCIN/AEI/10.13039/501100011033 under grant PID2020-117971GB-C22

²Partially supported by the Spanish project PID2019-105093GB-I00 and by the ICREA Acadèmia programme

A DNN that generalizes will perform well on test data on which it has not been trained. This is usually measured by the generalization gap, which is defined as the difference between the accuracy in training vs. test datasets. Although the two accuracies are correlated to a certain extent, studying training performance alone can be misleading. Several papers show how neural network performances on unseen examples can differ with respect to their training performances due to many reasons [1, 2, 3]. *To what extent is it possible to predict the generalization gap without testing a model?* In a practical sense, a measure of generalization that does not require a testing dataset eliminates the responsibility of maintaining and curating such a dataset. + *The main goal of this paper is to design a theoretical framework for the analysis of DNN neuron interactions and to obtain a generalization measure by approximating the generalization gap without the need of a testing set.*

The issue of finding a generalization measure has been explored extensively and a recent challenge on the topic provides an excellent framework for algorithmic benchmarking [4]. However, the most competitive participant methods rely on internal representations of independent layers, discarding more global structures that may be created across the network [5, 6] or even discarding structure altogether [7].

An alternative approach is provided by topological data analysis (TDA), an applied branch of algebraic topology that studies the shape of sets of points endowed with a metric structure. Such shapes are described by means of *persistence diagrams* [8], which are built on homological features of simplicial complexes constructed from the given dataset.

In this paper we present an approach to analyze persistence diagrams based on neuron interactions in deep neural networks. For this purpose, we use weighted graphs computed from activation correlations between neurons after training a network with a dataset. We compare the performance of different topological summaries from which the generalization gap can be regressed, and we find that a suitable combination of such summaries yields competitive results on measuring the generalization gap. Moreover, we show that topological summaries separate neural network architectures into clusters related with their generalization capacity.

The paper is structured as follows: in Section 2 we discuss related work; in Section 3 we define functional graphs and describe their topological summaries; in Section 4 we present and discuss experimental results, and conclusions are written down in Section 5. Supplemental material is provided in an appendix.

2. Related Work

Predicting generalization. Methods to predict the capacity of a model to generalize can be based on the following.

Theory. Bounds on the generalization gap fall in this category [9, 10, 11, 12]. Examples include the Vapnik–Chervonenkis dimension [13], measures based on spectral norms [14] or other norms of the weight tensors [15]. Generally, these methods rely on coarse-grained details about the networks that are not usually enough to obtain optimal performances.

Optimization. They might take into account the amount of epochs until a desired loss function [16, 17] or gradient noise is reached during training [18, 19, 20]. Unfortunately, both of these require knowledge of the training process, which might not be readily available.

Output. As a matter of example, competitive results were obtained in [21] with measures based on the distribution of the decision margin.

Sharpness. The key idea is to test the robustness of the network’s accuracy with respect to weight perturbation. There are a number of methods in this family, depending on whether the effect of perturbation is measured on average or in the worst case scenario, whether the perturbations are additive or multiplicative, and how the effect of perturbation is interpreted to predict generalization [22]. A variant is to test the robustness to input perturbations that preserve semantic content [7].

Internal representation. They deal with representations of input data in concrete layers of the network [5, 6]. The generalization gap is predicted by checking the robustness of the internal representations to separate the input data according to its labels.

Our approach obtains state-of-the-art performance when predicting generalization gap compared with methods in [4, 23]. Moreover, our procedure does not require a strong knowledge about the training process nor the dataset at hand.

Topological Data Analysis. TDA has had a number of applications in deep learning, such as studying the evolution of the input data’s topology through a network [24], or the topology of neuron activations themselves [25]. It has also been used as a method to reduce the size of the training resources without much loss in performance [26]. The use of TDA techniques for the analysis of weighted networks was also proposed in the context of network embeddings [27].

Along others such as [28] or [29], our work falls in the category of building and understanding relationships between neurons with the intent of predicting generalization. More specifically, we follow the steps initiated in [30] by formally defining the mathematical elements provided therein and studying more in depth their significance in terms of persistence summaries as well as their interpretability. This consolidates a technique that is general enough to study any network.

Other topological approaches have been used to gain insights with respect to model generalization. In [31], the authors perform a similar, more restrictive, construction of a graphical activation structure of neural networks to obtain persistent homology features of dimension 0. They show that these features are descriptive enough to undertake classification tasks and to detect adversarial examples using SVM models. Additionally, they use similar techniques to distinguish between adversarial and unaltered inputs when fed to a DNN [32]. Later research [33] based on [31] uses similar constructions to define a topology-based metric called *topological uncertainty*, that measures how similarly an unseen example activates DNN neurons with respect to the training dataset. Then, they use this metric to successfully perform model selection, outlier detection and shifted input detection.

We include a comparative analysis of a number of topological summaries with respect to their capacity to predict the generalization gap. This allows us to select the more robust, better-performing summaries with the objective of determining which properties of persistence diagrams are most relevant to a DNN’s generalization capacity.

3. Methodology

In this paper, we are interested in gleaming information about the dynamic behaviour of a trained neural network, i.e., the internal representations, structures and relationships between neuron activations during classification. In our context, the network behaves dynamically only in the presence of input data, forming a graph of neuron activations.

Our first goal is to define a mathematical structure describing the activation of a network when fed with a specific dataset \mathcal{D} consisting of pairs (x, y) where x and y represent inputs and

ground truth annotations respectively. To do so, we use a complete weighted graph whose set of vertices is in bijective correspondence with the set of neurons of the given network. Each vertex in this graph is represented by an *activation vector* of dimension $|\mathcal{D}|$ where the vector components are the activations for all $(x, y) \in \mathcal{D}$ corresponding to the neuron associated with the vertex via the bijection. Edges are weighted by a correlation distance between the activation vectors that they are connecting.

From this weighted graph we build a filtered simplicial complex computed from the edge weights. The topological features of this filtered simplicial complex are described by a *persistence diagram*, from which we extract suitable summaries with the purpose of explaining the generalization gap. The *accuracy* of a trained network is the percentage of correctly classified inputs, and the *generalization gap* is defined as the difference between the accuracy on the training dataset and the accuracy on the test set.

3.1. Network functional graphs

Let $V = \{v_1, \dots, v_n\}$ be the set of non-input nodes of a neural network N trained with a dataset $\mathcal{D} = \{(x, y)\}$, where x denotes inputs and y denotes corresponding values from a set of labels. For a node $v \in V$, we denote by $N_v(x)$ the activation of v on some input x , and define the *activation vector* of v as

$$A_v(\mathcal{D}) = (N_v(x))_{(x,y) \in \mathcal{D}}.$$

The set $A_N(\mathcal{D}) = \{A_v(\mathcal{D}) \mid v \in V\}$ of activation vectors is meant to capture the role of each node of N during inference.

A *distance* between two nodes $v_i, v_j \in V$ is defined as

$$d(v_i, v_j) = 1 - |\text{corr}(A_{v_i}(\mathcal{D}), A_{v_j}(\mathcal{D}))|, \quad (3.1)$$

where corr is the Pearson correlation coefficient. Although this function d does not satisfy the axioms in the definition of a metric, it is perfectly suitable for the application of techniques from TDA; see Appendix A for a discussion of this fact.

Nodes with constant activations can be safely regarded as not affecting the behaviour of the model, but rather its structure as a bias. Therefore, nodes with zero variance are discarded.

The complete weighted graph with vertices the nodes in V with nonzero variance and weights $d(v_i, v_j)$ on the edges will be called the *functional graph* of the trained neural network N . This graph encodes the functional behaviour of N . In this article we use Vietoris–Rips filtrations associated with the distance matrix $(d(v_i, v_j))$ from the functional graph for a homological persistence study, as defined in the next section.

3.2. Topological Data Analysis

3.2.1. Persistence diagrams

An *abstract simplicial complex*, a basic tool of algebraic topology, is a finite collection of sets S such that if $\alpha \in S$ and $\beta \subseteq \alpha$ then $\beta \in S$. Each abstract simplicial complex K determines a sequence of *homology groups* $H_n(K)$ for $n \geq 0$, generated by linearly independent n -dimensional cycles modulo boundaries. In this article coefficients of homology groups are meant in the field \mathbb{F}_2 of two elements.

If V is a finite set equipped with a distance function d , then for each subset $\alpha \subseteq V$ we may consider the *diameter* $\text{diam}(\alpha) = \max_{i,j \in \alpha} d(i, j)$ of α relative to d . The *Vietoris–Rips complex* of V at a parameter value $r \geq 0$ is an abstract simplicial complex defined as

$$\text{VR}_r(V) = \{\alpha \subseteq V : \text{diam}(\alpha) \leq 2r\}.$$

The set $\{\text{VR}_r(V)\}_{r \geq 0}$ is a nested collection of simplicial complexes, as $\text{VR}_r(V) \subseteq \text{VR}_s(V)$ if $r \leq s$. Each such filtration yields a *persistence diagram* for every integer $k \geq 0$, which contains a point (r, s) for each homology generator of dimension k born at a parameter value r and vanishing at s , where $r < s$. Further details about persistence diagrams can be found in [8].

3.2.2. Persistence summaries

There is a variety of numerical or vector-valued functions defined on persistence diagrams available for statistical analyses. We refer to such functions as *persistence summaries* or *descriptors*. In this subsection we present the summaries that have been used in our work.

Average births and average deaths. Since birth parameters and death parameters of homology generators do not yield linear models in general, different combinations of them have been explored, including their squares and the transformation $1/x + \ln x$ applied element-wise. The variance of births and deaths is also related with the generalization capacity of a network.

Average life and average midlife. The *life* or *lifetime* of a point (b, d) in a persistence diagram is defined as $d - b$, while the *midlife* is $(b + d)/2$. Average lives and average midlives yield good results when predicting generalization gap using linear extrapolations. These summaries have been used previously with a similar purpose in [34]. Other statistical descriptors such as standard deviation or variance of lives and midlives work equally well or better.

Lives and midlives yield nonlinear models too. For this reason, we have used lives and midlives directly and as a vector concatenation of them with their squares. This technique is based on the heuristic that the generalization gap of a network is highly influenced by the average position and dispersion of the points in a persistence diagram.

Persistent entropy. The definition of persistent entropy is an adaptation of the concept of entropy used in information theory, which, according to [35], provides a measure of the uncertainty of some random variable. The *entropy* of a persistence diagram P is defined as

$$\epsilon(P) = - \sum_{(b,d) \in P} ((d-b)/L) \log_2((d-b)/L), \quad (3.2)$$

where $L = \sum_{(b,d) \in P} (d-b)$. If one defines a discrete random variable that picks points (b, d) from P weighted according to their life, then the persistent entropy corresponds to the entropy of this random variable. This choice of weights is based on the assumption that points near the diagonal carry less information. Further details about persistent entropy can be found in [36].

Persistence pooling vectors. Persistence pooling vectors were introduced in [37] in order to improve a max-pooling procedure using TDA. This approach consists of analyzing only the most important points in a given persistence diagram, where importance is weighted according to the difference $d - b$. We define the n -th persistence pooling vector as the vector in descending order of the n maximum life values. If the persistence diagram has less than n points, then the void vector components are set to 0. We selected the highest 10 life values. This number has been chosen experimentally in view of the lack of score performance observed when selecting a larger number of vector components.

Complex polynomials. The topological summary introduced in [38] transforms persistence diagrams into polynomials with coefficients in the field \mathbb{C} of complex numbers whose roots are the images of persistence diagram points under a well-chosen $\mathbb{R}^2 \rightarrow \mathbb{C}$ mapping. In our study we used the transformation T defined in [38], although the choice of an optimal function remains a matter of study.

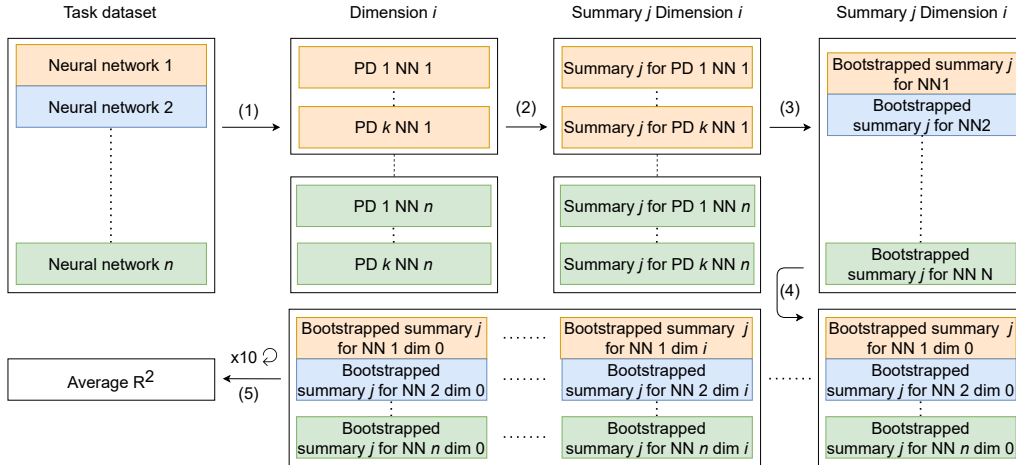


Figure 4.1: Experimental evaluation pipeline. Here *PD* and *NN* stand for persistence diagram and neural network, respectively. (1) Using sampling in CIFAR10/SVHN datasets and in the vertices of functional graphs to generate k different persistence diagrams per DNN and dimension; in our case, $k = 20$. (2) Computation of topological summaries using each persistence diagram of dimension i ; in our experiments, i takes values 0 and 1. (3) Bootstrapping per each group of summaries computed from the same DNN per each dimension (bootstrapping of each box for each different summary). (4) For each summary we generate X values concatenating dimensions. (5) For each combination of dimensions, we train a linear regression to predict the generalization gap taking 70% of the summaries randomly for the training set and computing R^2 with the other 30% of the dataset. We repeat these experiments 10 times and we assign the average of the 10 experiments as the final R^2 score.

4. Results

In the first part of this section we describe experimental setups and comment on computational complexity (Subsection 4.1). In the second part we evaluate our approach and discuss results (Subsection 4.2).

4.1. Experiments

Datasets. To compare performance, we use the dataset of trained DNNs provided by a NeurIPS 2020 competition [4]. The dataset is divided into nine tasks, each one composed by several neural network architectures trained to provide different generalization gaps on a particular dataset. We focus on the first two tasks, which were public when the competition was launched. The first task is composed of 96 VGG-like [39] neural networks, with a varying number of convolutional and dense layers (i.e., between 2 and 6 per layer type), trained on the CIFAR10 dataset [40]. The CIFAR10 dataset consists of 60,000 32×32 color images (3 channels) in 10 classes, representing vehicles (airplanes, automobiles, ships and trucks) and animals (birds, cats, deers, dogs, frogs and horses). The second task is composed of 54 neural networks with *network in network* architectures [41], with a varying number of blocks, trained on the SVHN dataset [42]. The SVHN is a digit classification benchmark dataset that contains 600,000 32×32 color images (3 channels) of printed digits (from 0 to 9, 10 classes) cropped from pictures of house number plates.

In all our experiments in each task, we randomly split the networks into 70% training and 30% test sets and repeat the experiment 10 times and average the scores.

Evaluation metrics. We use R^2 scores to evaluate how well the generalization gap is predicted by persistence summaries. As explained in Appendix B, the determination score R^2 can take negative values on a test set if a regression model works worse than a horizontal line. This indicates that a model adjusted with a set of training data is definitely wrong when applied to an unexplored dataset.

Experimental procedure. We generate for each neural network 20 persistence diagrams—see Section 4.1.1 for sampling details—of dimensions 0 and 1. Persistence summaries are computed per dimension and network using bootstrapping on each group of 20 persistence diagrams, extracted from the same network, of the given dimension. The bootstrapping process is performed with a sample size of 20 elements with replacement and 5 iterations directly over the different summaries computed from the 20 persistence diagrams. Then, to predict the generalization gap, we tune a linear regression on the training set per summary and task. Finally, we compute the R^2 score on the test set. The experimental evaluation pipeline is illustrated in Fig. 4.1.

4.1.1. Reducing computational complexity

Computational complexity. If $|\mathcal{D}|$ denotes the number of input samples for a dataset \mathcal{D} and $|V|$ is the number of nodes in a neural network N , then the set of activation vectors of nodes in N for the dataset \mathcal{D} has cardinality $|A_N(\mathcal{D})| = |\mathcal{D}| \times |V|$ (see Section 3.1 for details). To obtain weights on functional graphs, activation vectors have to be computed. These computations require either a huge quantity of memory or huge computational resources. Additionally, the complexity of algorithms for computing persistent homology is $O(n^3)$ if n is the number of simplices of the Vietoris–Rips complex and Gaussian elimination is used to find ranks of matrices of boundary operators, or $O(n^\omega)$ where ω is the exponent of matrix multiplication (currently 2.3729) if sparsity of boundary matrices is taken into account, as in [43]. In its turn, the number of simplices n depends cubically on the number $|V|$ of vertices of the functional graph if persistence diagrams are drawn in homological dimensions 0 and 1 only, which requires determination of simplices up to dimension 2. In practice, this limits persistence diagram computations to a few thousand vertices. In order to alleviate these problems in neural networks with millions on neurons, we introduce sampling strategies of both the input space and the functional graphs.

Sampling the input space. We compute activation vectors A_v for a fixed subsample $\mathcal{D}' \subseteq \mathcal{D}$. In order to justify that this subsampling does not affect the results of the analysis, it is enough to verify that $\text{corr}(A_{v_i}(\mathcal{D}'), A_{v_j}(\mathcal{D}'))$ is sufficiently close to $\text{corr}(A_{v_i}(\mathcal{D}), A_{v_j}(\mathcal{D}))$, and that small variations in the correlation coefficients produce small changes in the persistence diagrams. Arguments to prove this are indicated in the Appendix. In practice, $|\mathcal{D}'|$ is fixed to 2,000, an experimentally selected size that is large enough to obtain sufficient precision.

Sampling the functional graph. Because of computational limitations, in the case of modern DNNs less than 1% of the nodes—a priori, a statistically insignificant sample size—can be included in the persistent homology calculation. To alleviate this, we sample nodes according to a notion of importance, following ideas introduced in [44] adapted to neurons on a neural network instead of inputs of the dataset. Thus, let \mathcal{D}' be some selected subsample of the training dataset. The *importance score* of a node $v \in V$ is defined as

$$I_v(\mathcal{D}') = |\{x \in \mathcal{D}' : N_v(x) = \max\{N_{v_i}(x) : v_i \in V\}\}|, \quad (4.1)$$

i.e., the amount of inputs from \mathcal{D}' for which the activation of v is the largest (or tied-to-largest) among the rest of the nodes. Note that a majority of nodes v will have $I_v(\mathcal{D}') = 0$. This is

equivalent to excluding these nodes from analysis, which is undesirable —not only because it is unclear how this will affect the application of TDA, but also because the amount of nodes with $I_v(\mathcal{D}') \neq 0$ might be low enough to severely constrain the size of a subsample. Thus, from I we construct a probability distribution P on V , artificially inflated to make sure that every element of V appears with nonzero probability. This probability $P(v)$ is defined as

$$\frac{I_v(\mathcal{D}')}{|\mathcal{D}'| + 1} \text{ if } I_v(\mathcal{D}') > 0, \text{ and } \frac{1}{(|\mathcal{D}'| + 1) \cdot |\{u \in V : I_u(\mathcal{D}') = 0\}|} \text{ otherwise.} \quad (4.2)$$

Specifically, we sample 3,000 nodes (without repetition) according to this probability distribution, and restrict our analysis to these nodes. This sampling is non-deterministic, and thus can be repeated a number of times to obtain n different subsamples V_1, \dots, V_n . Applying the same transformations on the n resulting functional graphs we obtain n different persistence diagrams per network. Then, we use bootstrapping over the n summaries (see 3.2.2) combining them into a single one. This last representation aims to approximate the persistence summary that would be obtained without sampling.

Table 1: Top three TDA summaries per task according to their respective R^2 values. Summary 1: Average and standard deviation of births and deaths. Summary 2: Average and standard deviation of births and deaths, and squared. Summary 3: Average births and deaths and squared plus average lives and midlives and squared.

Task 1		
Top TDA summaries	Best dim	R^2 score
Summary 2	0 and 1	0.8663
Summary 1	0 and 1	0.7707
Summary 3	0 and 1	0.7317
Task 2		
Top TDA summaries	Best dim	R^2 score
Summary 3	0	0.9115
Summary 1	0 and 1	0.9109
Summary 2	0 and 1	0.9073

4.2. Discussion

Explainability. The TDA summaries that yielded the top three R^2 scores for the generalization gap prediction experiment are shown in Table 1. Basic statistical descriptors related to births and deaths of homology generators obtained highest scores overall. In particular, the vectors composed of averages and standard deviations of births and deaths (and their squares) were the ones that obtained best R^2 scores in both tasks. Figure D.1 in the Appendix shows the performance of the whole list of summaries. These results suggest that the generalization gap is mostly linked with the average position and dispersion of points in persistence diagrams. Summaries based on alleged predominance of larger lifetime values, such as persistent entropy or persistence pooling vectors, showed a lower predictive value.

A reason why the distribution of points in persistence diagrams of functional graphs is related with performance of networks could be the following. Generators of the 0-homology group of

a Vietoris–Rips simplicial complex at filtration level t correspond to groups of neurons in the functional graph in which every edge has a weight smaller than or equal to t , hence a correlation coefficient of $1 - t$ in absolute value among the neurons in the group. Thus, *the distribution of points in a 0-dimensional persistence diagram describes the degree of isolation vs. cooperation of active neurons in the network*. Diagrams with a concentration of points with low death values represent trained networks where neurons are highly correlated overall.

We found that the trend of the association between activation groups of neurons and generalization gap may depend on the architecture of the network. After training a network with a dataset, persistence summaries computed from samples of the same data or from similar datasets show a consistent association with the generalization gap in the same network or in networks with a closely related architecture. Yet, the sign of the correlation can be different when using other network models.

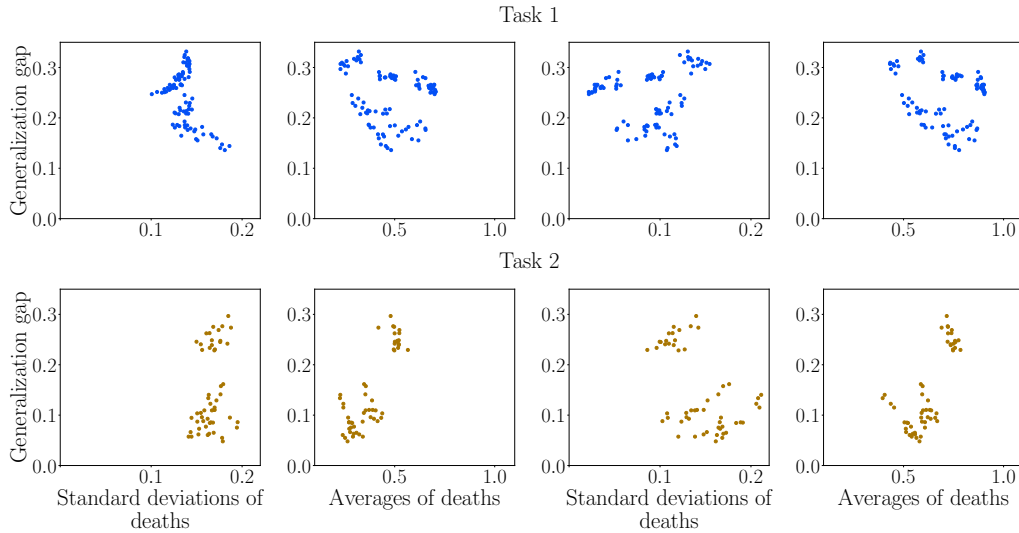


Figure 4.2: Standard deviations and averages of deaths for persistence diagrams in dimension 0 (first two columns) and 1 (last two columns) for tasks 1 and 2. For task 1, points represent 96 VGG-like neural network trained on the CIFAR10 dataset. For task 2, points correspond to 54 *network in network* architectures trained on the SVHN dataset.

The explainability capacity of TDA is further demonstrated in Fig. 4.2. For both task 1 and task 2, the different network architectures used in the experiments visibly fall into well-defined clusters. Hence, persistence summaries may serve to distinguish between types of networks in terms of their generalization gaps.

The patterns observed in Fig. 4.2 are cluster-wise consistent: the relationship between generalization gap and averages of deaths is inverse within each cluster, while the relationship between generalization gap and standard deviations of deaths is direct in a majority of clusters. This provides a possible explanation of the fact that averages and standard deviations of births or deaths were not found to be consistently correlated with the generalization gap, since some of the direct or inverse associations depicted in Fig. 4.2 reverse their sign when the separation into clusters is not taken into account.

We further analyzed if persistence diagrams for individual labels in a classification task were different between them to gain insights about what was influencing TDA methods and functional

graphs the most. We computed persistence diagrams in dimensions 0 and 1 per different neural network and per label. The datasets used to recreate functional graphs were restrictions of the test set to each label. Similar results were seen when comparing these persistence diagrams with the original ones. The majority of class-dependent persistence diagrams whose DNNs obtained extreme accuracies, i.e., highest and lowest, were analogous to the diagrams in the corresponding class-independent case. This shows that functional graphs are robust to unbalanced datasets in terms of the number of samples per label. Details and figures can be found in Appendix E.

Table 2: Average R^2 for task 1 and task 2. Comparing our best performing summaries with state of the art.

	Task 1	Task 2
Interpex	-0.1439	0.9776
Always Generalize	0.9715	0.8888
BrAIn	0.4079	0.6169
Ours	0.8663	0.9115

Topological summaries. Results show that linear models of persistence summaries can predict the generalization gap without the need of using multivariate models. We obtained competitive results in both tasks, as seen in Table 1 and Table 2. However, the fact that a summary based on a combination of non-linear transformations of persistence features yielded the best score for task 2 suggests that more complex models can have better capacity to relate persistence summaries with the generalization gap.

When it comes to ranking summaries, persistence pooling and persistent entropies produced the lowest R^2 scores overall. In fact, the features described by these summaries are fundamentally different from those of the other summaries, as both methods rely only on persistence values of points in the corresponding diagrams. Our results indicate that these values are not capable of accurately predicting generalization gap, in contrast with summaries based on location and distribution of points in persistence diagrams.

State-of-the-art comparison. Table 2 shows a comparison of the results of our best performing linear models based on persistence summaries with state-of-the-art methods. In this table, the R^2 scores describe the capacity of each method to predict the generalization gap with respect to the coefficient of determination. Our results are stable across both tasks while providing a more flexible framework to explain generalization.

5. Conclusions

We have defined a framework that can be used to explore interpretability of DNNs based on topological properties of their functional graphs. This relaxes the problem of understanding the internal representations of a neural network to, in a broad sense, understanding their *shape*. Regarding generalization, we have shown examples of how one can interpret DNN neuron interactions based on their correlations by means of persistence diagrams. Moreover, we proved that the generalization gap can be consistently predicted using topological persistence summaries extracted from functional graphs, with a competitive prediction accuracy on two different computer vision problems. The most successful summaries were those related with the average location and dispersion of points in persistence diagrams. Hence, it is not true in our case that points

near the diagonal in persistence diagrams are irrelevant. A more fine-grained analysis of TDA summaries would be needed to fully grasp the information provided by persistence diagrams.

Limitations. A practical limitation of persistent homology comes from its computational complexity—sampling methods are not necessarily optimal and information might be lost in sampling processes for datasets and for neurons. Transformations of persistence diagrams into summaries may also cause a loss of information; however, this seems unavoidable if one wants to obtain easy-to-compute generalization measures.

Future work. Although we found strong patterns relating persistence summaries with generalization gaps (Fig. 4.2), broader experimentation is required to see if these patterns are consistent among other kinds of networks and machine learning tasks, and also to make more explicit which features of the networks are involved in the TDA-driven clustering effect that we have observed.

Moreover, the mere definition of functional graphs raises a question: which is the optimal metric to compare neurons given an architecture? There might be better alternatives to linear correlation; for instance, Spearman correlation was used in co-activation graphs for a similar purpose in [45].

Another problem is to find an optimal neuron sampling strategy. This is related with the problem of finding the most relevant neurons in a DNN graph. Persistence summaries suggest that grouping neurons in terms of their activation structure is feasible for DNNs. However, understanding which functional phenomena are being captured into such communities of nodes needs further study. This could lead to the discovery of new architectural properties useful to develop better networks.

References

- [1] A. Azulay, Y. Weiss, Why do deep convolutional networks generalize so poorly to small image transformations?, *Journal of Machine Learning Research* 20 (2019) 1–25. [2](#)
- [2] I. J. Goodfellow, J. Shlens, C. Szegedy, Explaining and harnessing adversarial examples, in: Y. Bengio, Y. LeCun (Eds.), 3rd International Conference on Learning Representations, ICLR 2015, San Diego, CA, USA, May 7-9, 2015, Conference Track Proceedings, 2015. [2](#)
- [3] C. Zhang, S. Bengio, M. Hardt, B. Recht, O. Vinyals, Understanding deep learning requires rethinking generalization, *Communications of the ACM* 64 (2021) 107–115. [2](#)
- [4] Y. Jiang, P. Foret, S. Yak, D. M. Roy, H. Mobahi, G. K. Dziugaite, S. Bengio, S. Gunasekar, I. Guyon, B. Neyshabur, NeurIPS 2020 competition: Predicting generalization in deep learning (2020). [arXiv:2012.07976](#). [2](#), [3](#), [6](#), [16](#)
- [5] C. Lassance, L. Béthune, M. Bontou, M. Hamidouche, V. Gripon, Ranking deep learning generalization using label variation in latent geometry graphs (2020). [arXiv:2011.12737](#). [2](#), [3](#)
- [6] P. Natekar, M. Sharma, Representation based complexity measures for predicting generalization in deep learning (2020). [arXiv:2012.02775](#). [2](#), [3](#)
- [7] S. Aithal K, D. Kashyap, N. Subramanyam, Robustness to augmentations as a generalization metric (2021). [arXiv:2101.06459](#). [2](#), [3](#)
- [8] H. Edelsbrunner, J. Harer, *Computational Topology – an Introduction*, American Mathematical Society, 2010. [2](#), [5](#)
- [9] G. K. Dziugaite, D. M. Roy, Computing nonvacuous generalization bounds for deep (stochastic) neural networks with many more parameters than training data, in: *Proceedings of the Conference on Uncertainty in Artificial Intelligence (UAI)*, Sydney, 2017. [2](#)
- [10] D. A. McAllester, Pac-bayesian model averaging, in: *COLT*, Vol. 99, Citeseer, 1999, pp. 164–170. [2](#)
- [11] V. Nagarajan, J. Z. Kolter, Generalization in deep networks: The role of distance from initialization, in: *Neural Information Processing Systems (NeurIPS) – Deep Learning: Bridging Theory and Practice*, 2017. [2](#)
- [12] B. Neyshabur, R. R. Salakhutdinov, N. Srebro, Path-sgd: Path-normalized optimization in deep neural networks, in: *Advances in Neural Information Processing Systems*, 2015, pp. 2422–2430. [2](#)
- [13] V. N. Vapnik, A. Y. Chervonenkis, On the uniform convergence of relative frequencies of events to their probabilities, in: *Theory of Probability and its Applications*, Springer, 1971, pp. 11–30. [2](#)
- [14] P. L. Bartlett, D. J. Foster, M. J. Telgarsky, Spectrally-normalized margin bounds for neural networks, in: *Advances in Neural Information Processing Systems*, 2017, pp. 6240–6249. [2](#)

- [15] B. Neyshabur, R. Tomioka, N. Srebro, Norm-based capacity control in neural networks, in: Conference on Learning Theory, 2015, pp. 1376–1401. [2](#)
- [16] M. Hardt, B. Recht, Y. Singer, Train faster, generalize better: Stability of stochastic gradient descent, in: M. F. Balcan, K. Q. Weinberger (Eds.), Proceedings of The 33rd International Conference on Machine Learning, Vol. 48 of Proceedings of Machine Learning Research, PMLR, New York, New York, USA, 2016, pp. 1225–1234. [2](#)
- [17] A. C. Wilson, R. Roelofs, M. Stern, N. Srebro, B. Recht, The marginal value of adaptive gradient methods in machine learning, in: Advances in Neural Information Processing Systems, 2017, pp. 4148–4158. [2](#)
- [18] P. Chaudhari, S. Soatto, Stochastic gradient descent performs variational inference, converges to limit cycles for deep networks, in: 2018 Information Theory and Applications Workshop (ITA), IEEE, 2018, pp. 1–10. [2](#)
- [19] J. Mellor, J. Turner, A. Storkey, E. J. Crowley, Neural architecture search without training, in: M. Meila, T. Zhang (Eds.), Proceedings of the 38th International Conference on Machine Learning, Vol. 139 of Proceedings of Machine Learning Research, PMLR, 2021, pp. 7588–7598. [2](#)
- [20] S. Smith, Q. V. Le, A bayesian perspective on generalization and stochastic gradient descent, in: International Conference on Learning Representations (ICLR), 2018. [2](#)
- [21] Y. Jiang, D. Krishnan, H. Mobahi, S. Bengio, Predicting the generalization gap in deep networks with margin distributions, ICLR, 2019. [arXiv:1810.00113](#). [2](#)
- [22] N. S. Keskar, D. Mudigere, J. Nocedal, M. Smelyanskiy, P. T. P. Tang, On large-batch training for deep learning: Generalization gap and sharp minima (2016). [arXiv:1609.04836](#). [3](#)
- [23] Y. Jiang, B. Neyshabur, H. Mobahi, D. Krishnan, S. Bengio, Fantastic generalization measures and where to find them, ICLR, 2020. [3](#)
- [24] D. Goldfarb, Understanding deep neural networks using topological data analysis (2018). [arXiv:1811.00852](#). [3](#)
- [25] G. Naitzat, A. Zhitnikov, L.-H. Lim, Topology of deep neural networks, Journal of Machine Learning Research 21 (184) (2020) 1–40. [3](#)
- [26] R. Gonzalez-Diaz, M. A. Gutiérrez-Naranjo, E. Paluzo-Hidalgo, Topology-based representative datasets to reduce neural network training resources (2021). [arXiv:1903.08519](#). [3](#)
- [27] I. Knyazeva, O. Talalaeva, Topological data analysis approach for weighted networks embedding, in: A. Antonyuk, N. Basov (Eds.), Networks in the Global World V. NetGloW 2020, Vol. 181 of Lecture Notes in Networks and Systems, Springer, Cham, 2021. [3](#)
- [28] R. B. Gabriellson, Topological data analysis of convolutional neural networks’ weights on images (2017). [3](#)
- [29] B. Rieck, M. Togninalli, C. Bock, M. Moor, M. Horn, T. Gumbsch, K. Borgwardt, Neural persistence: A complexity measure for deep neural networks using algebraic topology, in: International Conference on Learning Representations, 2019. [3](#)
- [30] C. A. Corneanu, M. Madadi, S. Escalera, A. M. Martinez, What does it mean to learn in deep networks? and, how does one detect adversarial attacks?, in: 2019 IEEE/CVF Conference on Computer Vision and Pattern Recognition (CVPR), 2019, pp. 4752–4761. [3](#)
- [31] T. Gebhart, P. Schrater, A. Hylton, Characterizing the shape of activation space in deep neural networks, in: 2019 18th IEEE International Conference On Machine Learning And Applications (ICMLA), 2019, pp. 1537–1542. [3](#)
- [32] T. Gebhart, P. Schrater, Adversary detection in neural networks via persistent homology (2017). [arXiv:1711.10056](#). [3](#)
- [33] T. Lacombe, Y. Ike, M. Carrière, F. Chazal, M. Glisse, Y. Umeda, Topological uncertainty: Monitoring trained neural networks through persistence of activation graphs, in: Z.-H. Zhou (Ed.), Proceedings of the Thirtieth International Joint Conference on Artificial Intelligence, IJCAI-21, International Joint Conferences on Artificial Intelligence Organization, 2021, pp. 2666–2672. [3](#)
- [34] C. A. Corneanu, M. Madadi, S. Escalera, A. M. Martinez, Computing the testing error without a testing set, in: 2020 IEEE/CVF Conference on Computer Vision and Pattern Recognition (CVPR), 2020, pp. 2674–2682. [5](#)
- [35] M. Mezard, A. Montanari, Information, Physics, and Computation, Oxford University Press, 2009. [5](#)
- [36] N. Atienza, R. Gonzalez-Diaz, M. Soriano-Trigueros, On the stability of persistent entropy and new summary functions for topological data analysis, Pattern Recognition 107 (2020) 107509. [5](#)
- [37] T. Bonis, M. Ovsjanikov, S. Oudot, F. Chazal, Persistence-based pooling for shape pose recognition, CTIC (2016) 19–29. [5](#)
- [38] B. D. Fabio, M. Ferri, Comparing persistence diagrams through complex vectors, in: Image Analysis and Processing – ICIAP 2015, Vol. 9279 of Lecture Notes in Computer Science, Springer, 2015. [5](#)
- [39] K. Simonyan, A. Zisserman, Very deep convolutional networks for large-scale image recognition, in: International Conference on Learning Representations, 2015. [6](#)
- [40] A. Krizhevsky, Learning multiple layers of features from tiny images, Tech. rep. (2009). [6](#)
- [41] M. Lin, Q. Chen, S. Yan, Network in network (2014). [arXiv:1312.4400](#). [6](#)
- [42] Y. Netzer, T. Wang, A. Coates, A. Bissacco, B. Wu, A. Y. Ng, Reading digits in natural images with unsupervised feature learning, in: NIPS Workshop on Deep Learning and Unsupervised Feature Learning 2011, 2011. [6](#)

- [43] N. Milosavljević, D. Morozov, P. Škraba, Zigzag persistent homology in matrix multiplication time, in: Proceedings of the 27th Annual Symposium on Computational Geometry (SoCG’11), 2011, pp. 216–225. [7](#)
- [44] E. Nezhadarya, E. Taghavi, R. Razani, B. Liu, J. Luo, Adaptive hierarchical down-sampling for point cloud classification, in: 2020 IEEE/CVF Conference on Computer Vision and Pattern Recognition (CVPR), 2020, pp. 12953–12961. [7](#)
- [45] V. A. C. Horta, I. Tiddi, S. Little, A. Mileo, Extracting knowledge from deep neural networks through graph analysis, *Future Generation Computer Systems* 120 (2021) 109–118. [11](#)
- [46] F. Chazal, V. de Silva, S. Oudot, Persistence stability for geometric complexes, *Geometriae Dedicata* 173 (2014) 193–214. [13](#), [14](#)
- [47] S. Chowdhury, F. Mémoli, A functorial Dowker theorem and persistent homology of asymmetric networks, *Journal of Applied and Computational Topology* 173 (2) (2018) 115–175. [13](#)
- [48] A. W. V. der Vaart, *Asymptotic Statistics*, Cambridge University Press, New York, 1998. [14](#)
- [49] S. Zhang, M. Xiao, H. Wang, Gpu-accelerated computation of vietoris-rips persistence barcodes, in: 36th International Symposium on Computational Geometry (SoCG 2020), Schloss Dagstuhl-Leibniz-Zentrum für Informatik, 2020. [16](#)
- [50] G. Tauzin, U. Lupo, L. Tunstall, J. B. Pérez, M. Caorsi, A. M. Medina-Mardones, A. Dassatti, K. Hess, giotto-tda: A topological data analysis toolkit for machine learning and data exploration, *Journal of Machine Learning Research* 22 (39) (2021) 1–6. [16](#)
- [51] P. Virtanen, et al., SciPy 1.0: Fundamental Algorithms for Scientific Computing in Python, *Nature Methods* 17 (2020) 261–272. [16](#)

Appendix

This appendix contains additional explanations and analyses related with some parts of the paper. In Appendix A we comment on the distance used to build functional graphs. In Appendix B we define and explain the coefficient of determination R^2 . In Appendix C we address the convergence of a sample correlation with respect to the number of elements in the sample —this is done in order to justify that the input space subsampling performed in the experiments does not affect the results of the analyses if the sample is big enough. In Appendix D we present results for the full collection of samples by means of a heatmap, and Appendix E contains an analysis per label of persistence diagrams in dimensions 0 and 1. Technical details about computer resources used in our study are provided in Appendix F.

Appendix A. Correlation distance in functional graphs

In Section 3.1 we defined functional graphs as unoriented weighted graphs whose edge weights are defined as

$$d(v_i, v_j) = 1 - |\text{corr}(A_{v_i}(\mathcal{D}), A_{v_j}(\mathcal{D}))| \quad (\text{A.1})$$

for a training dataset \mathcal{D} , where corr denotes the Pearson correlation coefficient. This function d is not a metric, since it can take a zero value on distinct nodes and the triangle inequality need not hold. However, Vietoris–Rips filtrations can be associated with arbitrary functions $X \times X \rightarrow \mathbb{R}$ where X is any set, and a form of stability holds in such generality [46, 47]. In our case, the suitability of (A.1) is implied by the next remarks.

1. Although d does not necessarily satisfy that $d(x, y) \neq 0$ whenever $x \neq y$, this does not affect persistent homology, since the matrix $(d(v_i, v_j))$ yields a Vietoris–Rips filtration homotopy equivalent to the one obtained by identifying two nodes x and y if $d(x, y) = 0$.
2. While d does not satisfy the triangle inequality, the following transformation does:

$$\tilde{d}(v_i, v_j) = \sqrt{1 - (1 - d(v_i, v_j))^2}. \quad (\text{A.2})$$

Since the function $\gamma(t) = \sqrt{1 - (1 - t)^2}$ is strictly monotonic on $[0, 1]$, d and \tilde{d} produce the same Vietoris–Rips filtrations, albeit at different thresholds. From this fact it follows that continuity of persistence diagrams under small displacements in the space of functional graphs holds for d . This is proved using persistence stability for metric spaces [46] together with the uniform continuity of γ on $[0, 1]$.

Appendix B. Determination score

In Section 4.1 we used the coefficient of determination R^2 as the evaluation metric of our experiments. It is defined as

$$R^2(y, \hat{y}) = 1 - \frac{\sum_{i=1}^n (y_i - \hat{y}_i)^2}{\sum_{i=1}^n (y_i - \bar{y})^2}, \quad (\text{B.1})$$

where y is the ordered set of actual values, \hat{y} is the ordered set of predicted values, and \bar{y} denotes the mean of y . This coefficient ranges from 0 to 1 on the training dataset but can be outside that range on unseen data. When the score is 1, our model perfectly predicts the values of y . On the other hand, if $R^2(y, \hat{y}) = 0$ then

$$\sum_{i=1}^n (y_i - \hat{y}_i)^2 = \sum_{i=1}^n (y_i - \bar{y})^2.$$

This score is obtained when one uses a horizontal line at the average of the set of y -values as a model. If a model performs worse than this (which usually indicates that the choice of model itself was ill-advised), then the numerator of (B.1) can grow arbitrarily large, and thus R^2 can be negative. If an R^2 value is negative, then the prediction is worse than ignoring the input and predicting the average of the sample. This can actually happen when the training set yields a model that does not generalize in the test set.

Appendix C. Convergence of sample correlation

In 4.1.1 we stated a way to sample the input space and claimed that $\text{corr}(A_{v_i}(\mathcal{D}'), A_{v_j}(\mathcal{D}'))$ is sufficiently close to $\text{corr}(A_{v_i}(\mathcal{D}), A_{v_j}(\mathcal{D}))$ when taking large samples. To justify this claim, let X and Y be two random variables with non-null variance, and, for each $n \in \mathbb{N}$, let X^n and Y^n denote sequences of n samples from X and Y , respectively. Then the sample correlation of X^n and Y^n converges in probability to the correlation between X and Y by the law of large numbers and the continuous mapping theorem [48].

Appendix D. Complete results for experiments

Complete results for the whole set of topological summaries used in the experiments of Section 4.1 can be found in Fig. D.1. These summaries consist of vectors obtained by applying transformations from 3.2.2 or a concatenation of them. Each summary was computed for dimensions 0 and 1, and linear models were trained for the same dimensions or for a concatenation of summaries of both dimensions. The chosen summaries were the following: (0) Persistence pooling of 10 elements. (1) Average lives and midlives. (2) Average lives and midlives, original and squared. (3) Average births and deaths. (4) Average births and deaths with a logarithmic model. (5) Average births and deaths, original and squared. (6) Combination of features (2) and (5).

(7) Persistent entropies. (8) Averages and standard deviations of births and deaths. (9) Averages and standard deviations of births and deaths, original and squared. (10) Complex polynomials of 10 coefficients.

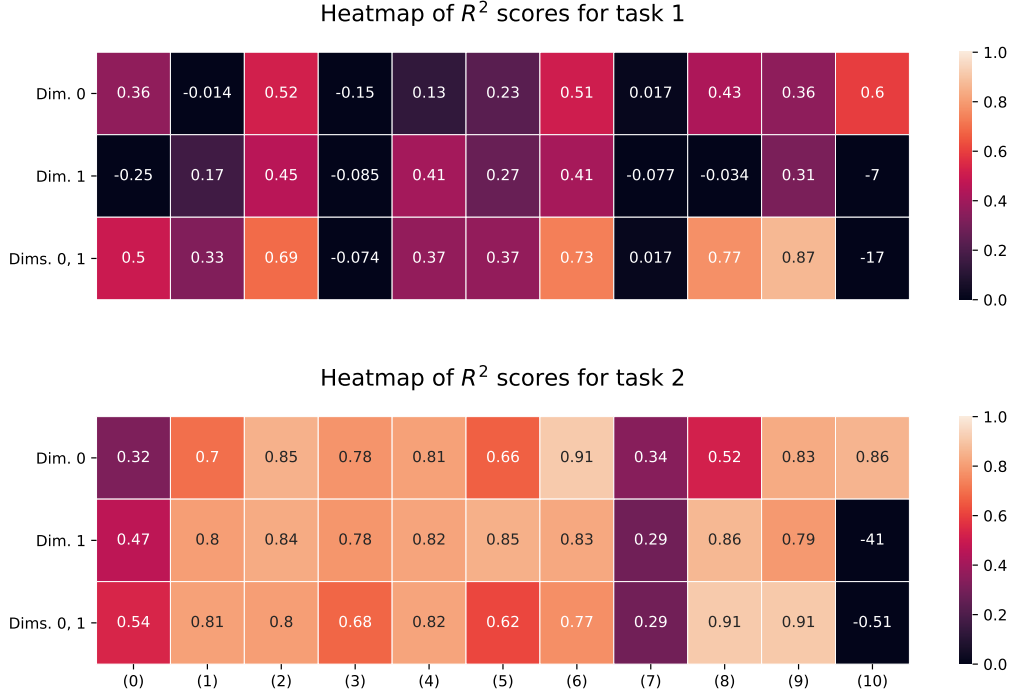


Figure D.1: Average R^2 scores for task 1 and task 2 from persistence diagrams of dimensions 0 and 1. Each column represents a topological summary: (0) Persistence pooling of 10 elements. (1) Average lives and midlives. (2) Average lives and midlives, original and squared. (3) Average births and deaths. (4) Average births and deaths with a logarithmic model. (5) Average births and deaths, original and squared. (6) Combination of features (2) and (5). (7) Persistent entropies. (8) Averages and standard deviations of births and deaths. (9) Averages and standard deviations of births and deaths, original and squared. (10) Complex polynomials of 10 coefficients.

As explained in Section 4, the TDA summaries that achieve highest R^2 scores for the generalization gap are those combining averages and standard deviations of births and deaths of homology generators. This fact is consistently observed and suggests that the generalization gap is predominantly linked with the average position and dispersion of points in persistence diagrams. Diagrams showing clusters of points with low death values represent neural networks where neurons tend to be highly correlated, while scattered points with a larger range of death values correspond to less collaborative structures.

Overall, results are more conclusive for task 2 than for task 1, and more significant in homological dimension 0, although the best R^2 scores are obtained when dimension 0 and dimension 1 are jointly taken into account. It should also be noticed that R^2 scores grow when squares of summaries are added to the model, suggesting departure from linearity.

Appendix E. Analysis on individual labels

This section shows detailed results of the experiments per label discussed in Section 4.2. We computed persistence diagrams of dimensions 0 and 1 per different neural network and per label, where the datasets used to recreate functional graphs were the restriction of the test sets to each label. We computed accuracy for each of these testing subsets, and plotted persistence diagrams corresponding to those neural networks that achieved the maximum and minimum accuracies on testing subsets per label for dimensions 0 and 1. The results can be seen in Figures E.1, E.2, E.3 and E.4. These results are consistent with what we found in persistence diagrams computed with the whole training dataset. Thus we see that distinction between inputs of different labels does not have a substantial influence on the distribution of points in persistence diagrams.

For a more convenient visualization, persistence diagrams in dimension 0 have been replaced with lifetime density curves, calculated by means of Gaussian kernels. Lifetime values are equal to death values for 0-homology generators.

It can be seen in Fig. E.3 and Fig. E.4 that increased accuracy values match with scattering of points downwards the diagonal of the persistence diagram in dimension 1 and with a lower average life in dimension 0, indicating higher correlations among neurons. However, this pattern is not consistent with other architectures, such as those used in task 1. This is partially explained by the splitting of network types into clusters as observed in Fig. 4.2.

Appendix F. Hardware, software and licenses

Persistence diagrams were computed with Python Ripser++ [49] (MIT License) using a Quadro P6000 GPU. Persistence summaries were computed with the giotto-tda framework [50] (AG-PLv3 License), and density curves were drawn using SciPy 1.8.0 [51]. Analysis was done using a personal computer with an Intel Core i7 (4th generation) processor with an NVIDIA GeForce GTX 960M 2GB GDDR5, using especially the libraries Jupyter Notebook (New BSD License), NumPy (BSD 3-Clause “New” or “Revised” License) and TensorFlow with Keras (Apache 2.0 License). An own Docker (Apache 2.0 License) image was used to compute persistence diagrams. The dataset of neural networks from [4] is licensed under Apache 2.0.

Minimum and maximum accuracy persistence diagrams of dimension 0 for task 1

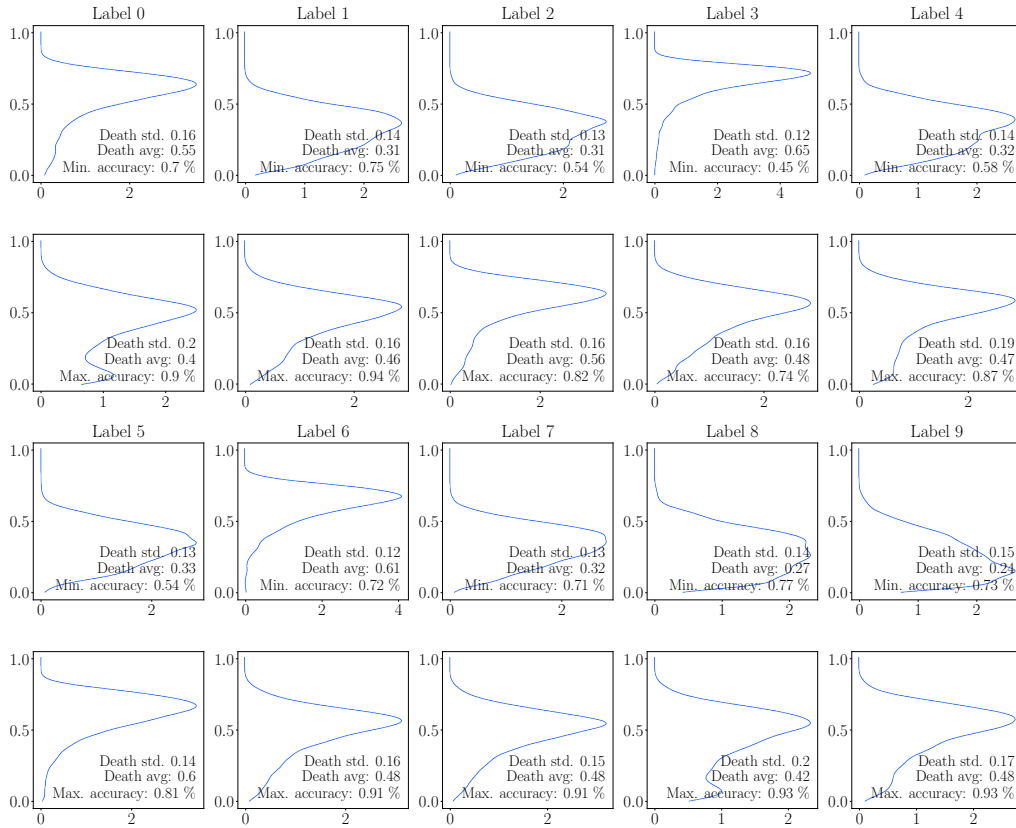


Figure E.1: Lifetime densities in persistence diagrams in homological dimension 0 of 96 VGG-like neural networks with minimum and maximum accuracies on the testing set per label for task 1.

Minimum and maximum accuracy persistence diagrams of dimension 1 for task 1

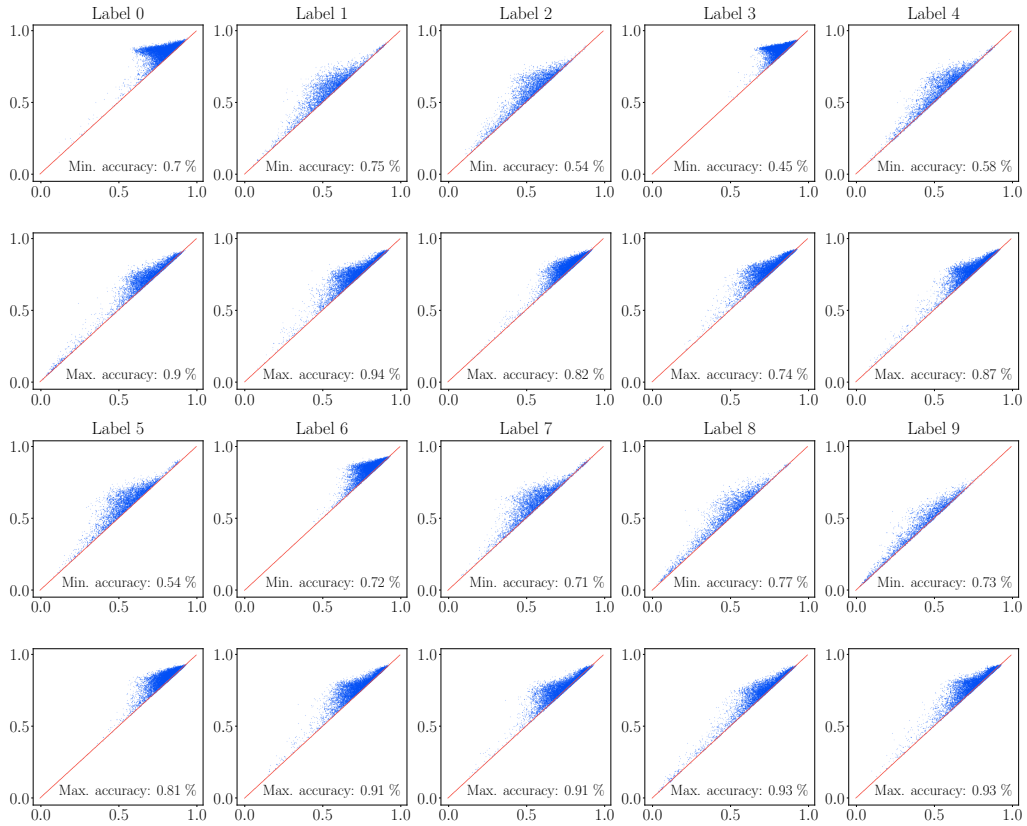


Figure E.2: Persistence diagrams in homological dimension 1 of 96 VGG-like neural networks with minimum and maximum accuracies on the testing set per label for task 1.

Minimum and maximum accuracy persistence diagrams of dimension 0 for task 2

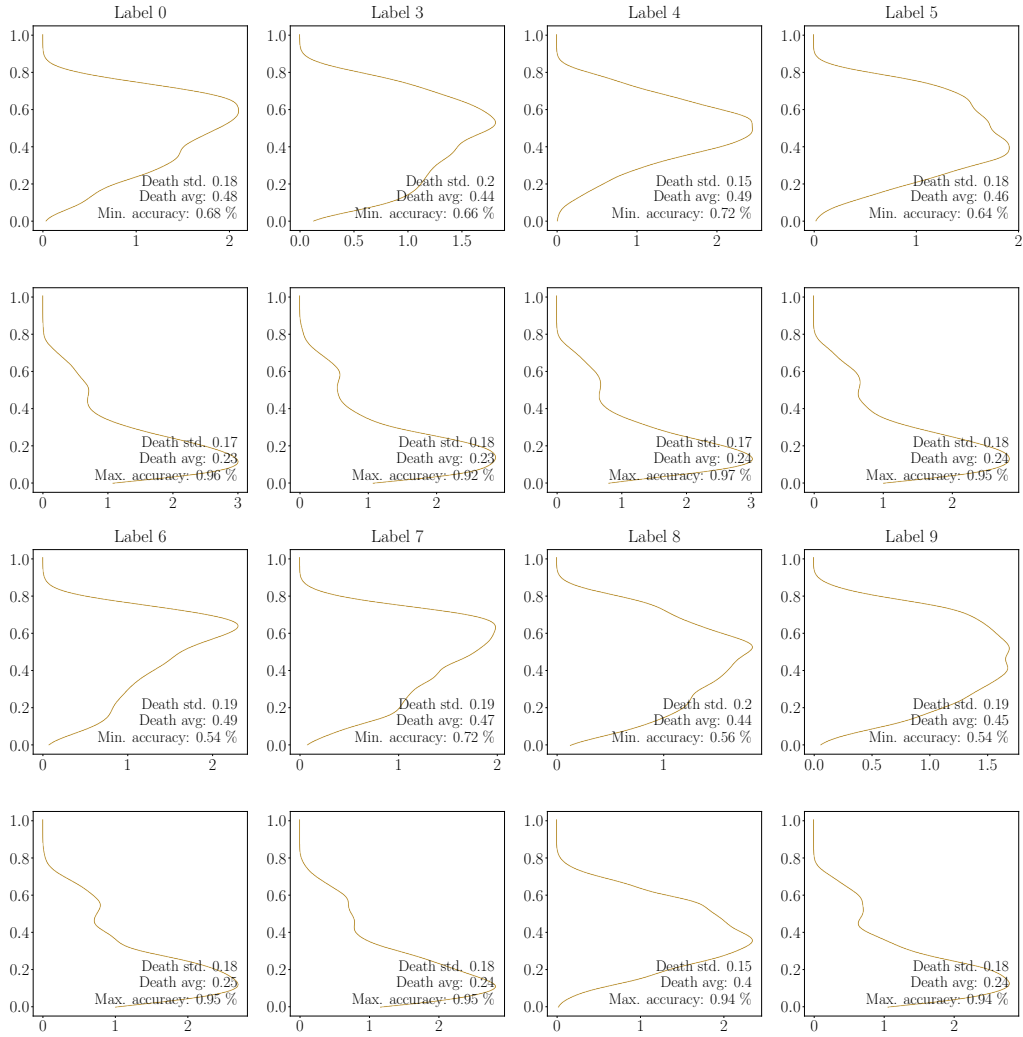


Figure E.3: Lifetime densities in persistence diagrams in homological dimension 0 of 54 *network in network* architectures with minimum and maximum accuracies on the testing set per label for task 2.

Minimum and maximum accuracy persistence diagrams of dimension 1 for task 2

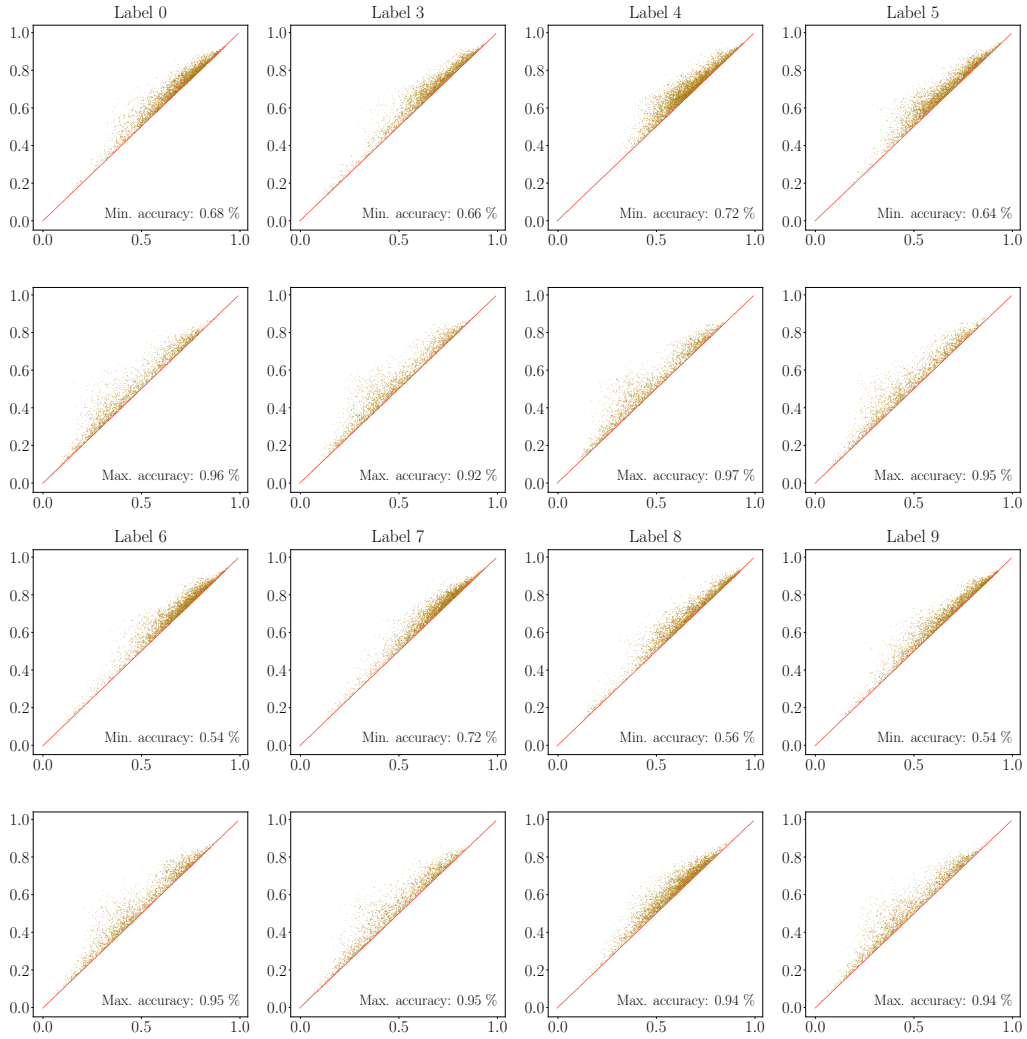


Figure E.4: Persistence diagrams in homological dimension 1 of 54 *network in network* architectures with minimum and maximum accuracies on the testing set per label for task 2.